ETMM 9

Thessaloniki | Greece

programme 6-8 JUNE 2012

Makedonia Palace
THESSALONIKI
Greece

European Research Community On Flow, Turbulence and Combustion

Organising Committee

Bernard Geurts (Chairman), University of Twente
Ananias Tomboulides, University of Western Macedonia
Dominic von Terzi, GE Global Research, Munich

Papers and Programme Committee

B.J. Geurts (Chairman)

J-P. Bonnet
S. Kassinos
B.E. Launder
M. Leschziner
W. Rodi
D. von Terzi
A. Tomboulides
J. Westerweel

Local Arrangements Committee

A.G. Tomboulides (Co-chairman and Local Organizer)

J. Bartzis
G. Bergeles
J. Ekaterinaris
G. Giannakoglou
A. Goulas
N. Markatos
N. Moussiopoulos
P. Prinos
J. Tsamopoulos
N. Vlachos

Scientific Advisory Committee

N. Adams (Germany)
V. Armenio (Italy)
B. Aupoix (France)
C. Bailly (France)
A. Boguslawski (Poland)
M. Braza (France)
Y.D. Choi (Korea)
P. Comte (France) († 2011)
L. Davidson (Sweden)
E. Dick (Belgium)
L. Djenidi (Australia)
C. Dopazo (Spain)
D. Drikakis (Cyprus)
S. Drobniak (Poland)
P. Durbin (USA)
J. Fort (Czech Republic)
R. Friedrich (Germany)
T. Gatski (USA)
K. Hanjalić (Italy)
S. Jakirlić (Germany)
J. Janicka (Germany)
J. Jimenez (Spain)
N. Kasagi (Japan)
J. Kuerten (Netherlands)
R. Manceau (France)
M. Manna (Italy)
F. Martelli (Italy)
J. Meyers (Belgium)
F. Menter (Germany)
T. Miyauchi (Japan)
B. Muller (Norway)
S. Obi (Japan)
R.V.A. Oliemans (Netherlands)
N. Peters (Germany)
U. Piomelli (Canada)
T. Poinsot (France)
J. Pozorski (Poland)
P. Sagaut (France)
N. Sandham (UK)
M. Savill (UK)
P. Schlatter (Sweden)
J. Sesterhenn (Germany)
A. Soldati (Italy)
P.R. Spalart (USA)
A. v. Steenhoven (Netherlands)
M. Strelets (Russia)
K. Suga (Japan)
D. Thevenin (Germany)
L. Vervisch (France)
R. Verzicco (Italy)

PROGRAMME

DAY 1 // JUNE 6, 2012

08.45 - 09.00:	**Welcome and orientation**	(ALEXANDROS II)
09.00 - 09.45:	Plenary: **LES of turbulent flows over multi-scale rough surfaces using a dynamic roughness model** Charles Meneveau (John Hopkins) Chairman: B. Geurts	(ALEXANDROS II)
09.45 - 10.30:	Plenary: **Large-scale Spectral Element based DNS of complex Turbulent flows** Paul Fischer (Argonne National Laboratories) Chairman: A. Tomboulides	(ALEXANDROS II)
10.30 - 10.50:	**Coffee Break**	(ALEXANDROS I)

10.50 - 12.30: **PARALLEL SESSIONS**

ALEXANDROS II	AMPHITRION I	AMPHITRION II
S1: LES Methods & Applications 1 Chairman: C. Meneveau	**S2: Hybrid RANS 1** Chairman: S. Jakirlic	**S3: Experiments 1** Chairman: A. Pollard
Large Eddy Simulation of Supercritical Fluid Flow Injection **PETIT X., RIBERT G., DOMINGO P.**	Hybrid RANS/LES of flow in a rib-roughened channel with rotation **KUBACKI S., ROKICKI J., DICK E.**	PIV and DNS analysis of viscoelastic turbulent flows behind a rectangular orifice **TSUKAHARA T., MOTOZAWA M., KAWASE T., TSURUMI D., KAWAGUCHI Y.**
Zonal Detached Eddy Simulation of the Dynamics of an Axisymmetric Separating/Reattaching Flow in Presence of Side-Cylinders **PAIN R., WEISS P., DECK S.**	A new Approach of Zonal Hybrid RANS-LES Based on a Two-equation k-ε Model **DAVIDSON L.**	A test facility for assessing simulations of jets in cross flow configurations **BRUEL P., FLORENCIANO J.-L., KOUSKSOU T., LEDERLIN T.**
Testing different advection schemes for coarse high-Re LES simulations of a jet in crossflow and weak coflow **DE WIT L., VAN RHEE C.**	Anisotropic linear forcing for synthetic turbulence generation in hybrid RANS/LES modelling **De LAAGE De MEUX B., AUDEBERT B., MANCEAU R.**	PIV Measurement and Force Estimation of the Flow Induced by a Heaving Elastic Plate **KATO K., OBI S.**

PROGRAMME

DAY 1 // JUNE 6, 2012

On the unsteady aerodynamics of road vehicles in the dynamic motions **CHENG S.Y., TSUBOKURA M., OKADA Y., NAKASHIMA T., NOUZAWA T., KOBAYASHI T.**	Hybrid RANS/LES and PANS computations of plane impinging jets **KUBACKI S., ROKICKI J., DICK E.**	Experimental and computational study of a wind flow over a hill covered with forest **AGAFONOVA O., MITYAKOV A., CHAUDHARI A., HAMALAINEN J.**
Application of r-adaptation to LES of turbulent flow **HERTEL C. , SCHUMICHEN M., FROHLICH J.**		Effect of the separation wall in the mixing properties of coaxial jets **TALAMELLI A., ORLU R., SEGALINI A.**
12.30 - 14.00: **Lunch Break**		

14.00 - 15.40: **PARALLEL SESSIONS**

ALEXANDROS II	AMPHITRION I	AMPHITRION II
S4: LES Methods & Applications 2 Chairman: B. Geurts	**S5: RANS Modelling** Chairman: A. Goulas	**S6: Experiments 2** Chairman: S. Obi
Large Eddy Simulation of wind turbine wakes **CHATELAIN P., BACKAERT S., WINCKELMANS G., KERN S.**	An explicit algebraic Reynolds stress and scalar flux model for stably stratified turbulent flows **LAZEROMS W.M.J., BRETHOUWER G., WALLIN S, JOHANSSON A.V.**	LDA measurements in the development region of low Reynolds Number Turbulent Pipe Jet **VOUROS AI., PANIDIS Th.**
Wall-modeled large-eddy simulation of transitional separated flow over an airfoil at high Reynolds number **ASADA K., KAWAI S.**	Effects of cross sectional shape on the motion of 3D turbulent gravity currents **M. TSAKIRI, KOFTIS T., PRINOS P., SOULIOTIS D.**	Application of PIV Technique for the Study of Turbulent Structure of Cavitating Flows around a NACA0015 Series Hydrofoil **ALEKSEENKO S.V., KRAVTSOVA A.Yu., MARCOVICH D.M., PERVUNIN K.S., TIMOSHEVSKIY M.V.**

HYBRID RANS/LES OF FLOW IN A RIB-ROUGHENED CHANNEL WITH ROTATION

S. Kubacki[1], J. Rokicki[1] and E. Dick[2]

[1]Institute of Aeronautics and Applied Mechanics, Warsaw University of Technology, Nowowiejska 24, 00-665 Warsaw, Poland
[2]Department of Flow, Heat and Combustion Mechanics, Ghent University, St.-Pietersnieuwstraat 41, B-9000 Ghent, Belgium

slawomir.kubacki@meil.pw.edu.pl

Abstract

The aim of the present study is to verify the reliability of a k-ω based hybrid RANS/LES model in reproducing the flow in a rib-roughened rotating channel. The numerical results obtained with the hybrid RANS/LES model are compared to experimental data by Coletti and Arts (2011) and to the results obtained with the RANS k-ω model of Wilcox (2008). We demonstrate that the hybrid RANS/LES model gives realistic results for simulation of the rotating ribbed duct flow, without the necessity to add ad hoc corrections for system rotation to the underlying RANS model.

1 Introduction

Proper accounting for rotational effects is very important in tubomachinery applications. The accurate determination of the flow characteristics in orthogonally rotating systems is relevant for analysis of the flow in blade passages of radial compressors and in the internal cavities of rotating turbine blades.

The monotonically integrated LES (MILES) has been employed by Lohasz et al. (2006) to study the flow details in ribbed stationary channel flow. The ratio of the rib size to the channel height was 0.3 and the Reynolds number based on the hydraulic diameter was set to Re=40,000. The analysis of the instantaneous flow field allowed observing spanwise oriented vortices close to the leading edge of the rib which further deformed into λ-shaped structures. These λ-shaped vortices were further entrained into the shear layer behind the rib. The work by Lohasz et al. (2006) demonstrated that a sufficiently low value of the Smagorinsky constant has to be specified for a successful simulation of ribbed channel flow.

The flow dynamics inside the ribbed channel significantly changes if the channel is subjected to rotation, as demonstrated in the LES study by Abdel-Wahab and Tafti (2004) and in measurements by Coletti et al. (2010) and Colleti and Arts (2011). Abdel-Wahab and Tafti (2004) employed the dynamic Smagorinsky model for calculation of the rib-roughened channel flow at various rotation velocities. The bulk Reynolds number was Re=20,000. The peak values of the turbulent kinetic energy differ by a factor of two in the boundary layers formed on the leading and trailing sides of the channel and the amplitude of small-scale fluctuations changed significantly with rotation close to the trailing side. In Coletti et al. (2010) and Colleti and Arts (2011) the influence of the Coriolis force was investigated experimentally using a PIV system which was put in rotation together with the channel. This allowed capturing the relative velocity field at high resolution. The ratio of the rib size to the channel height was 0.1, and the Reynolds number was 15,000. Rotation in both clockwise and counter-clockwise directions was considered. In clockwise rotation, Kelvin-Helmholtz rollers were produced in the separated shear layer behind the rib owing to the stabilising effect of the forces. This led to a much longer separation bubble behind the obstacle with respect to the length measured in the stationary channel. In counter-clockwise rotation, a small separation bubble was formed at the leading edge of the rib which reattached very quickly at the top of the rib. Further downstream, a three-dimensional turbulent motion was created due to the destabilising effect of the forces. This led to a shorter length of the separation bubble behind the rib with respect to one reported in the non-rotating case. In the present work, numerical results obtained with a k-ω RANS and a k-ω based hybrid RANS/LES model are compared to the experimental results by Colleti and Arts (2011).

The hybrid RANS/LES model studied here belongs to the class of unified DES-type models. In LES mode, the hybrid model uses two definitions of the local grid size. One is the maximum distance between the cell faces in the destruction term of the turbulent kinetic energy equation and the other is the cube root of the cell volume in the eddy-viscosity formula. This allows for better accounting for flow inhomogeneity on anisotropic grids. Under the assumption of local equilibrium, the eddy viscosity of the hybrid model reduces to a Smagorinsky subgrid viscosity with the usual constant C_s=0.1. In RANS mode, the hybrid model switches into the newest version of the k-ω model by Wilcox (2008).

2 Mathematical formulation

For a constant-density fluid, the continuity and momentum equations take the following forms in a frame subjected to rotation

$$\frac{\partial \overline{u}_i}{\partial x_i} = 0 \tag{1}$$

$$\frac{\partial \overline{u}_i}{\partial t} + \frac{\partial (\overline{u}_i \overline{u}_j)}{\partial x_j} = -\frac{1}{\rho}\frac{\partial \overline{p}}{\partial x_i} + \frac{\partial}{\partial x_j}(\sigma_{ij} + \tau_{ij}) - \frac{1}{\rho}\frac{\partial P}{\partial x_1}\delta_{1i} + 2\varepsilon_{ij3}\Omega \overline{u}_j \tag{2}$$

The overbars in (1) and (2) denote ensemble averaged quantities in RANS regions and filtered quantities in LES regions of the hybrid model $\sigma_{ij} = 2\nu \overline{S}_{ij}$ and $\tau_{ij} = 2\nu_t \overline{S}_{ij} - 2/3 k\delta_{ij}$ denote the components of the molecular viscous and the modelled stress tensors, respectively, with ν the kinematic molecular viscosity, ν_t the turbulent/subgrid viscosity and $\overline{S}_{ij} = 1/2(\partial \overline{u}_i / \partial x_j + \partial \overline{u}_j / \partial x_i) - 1/3(\partial \overline{u}_k / \partial x_k)\delta_{ij}$ the components of the shear rate tensor. $\overline{p}$ denotes the effective pressure, which is a part of the pressure combined with the potential energies associated to gravity and centrifugal force. $\partial P / \partial x_1$ represents the mean pressure gradient imposed in the streamwise direction of the periodic domain, adjusted to guarantee the correct mass flow rate at each time step, ε_{ijk} is the Levi-Civita symbol and Ω is the angular velocity.

The transport equations of the hybrid RANS/LES model are

$$\frac{\partial k}{\partial t} + \frac{\partial (\overline{u}_j k)}{\partial x_j} = \tau_{ij}\frac{\partial \overline{u}_i}{\partial x_j} - \max\left(\beta^* k\omega, \frac{k^{3/2}}{C_{DES}\Delta}\right) + \frac{\partial}{\partial x_j}\left[\left(\nu + \sigma^* \frac{k}{\omega}\right)\frac{\partial k}{\partial x_j}\right], \tag{3}$$

$$\frac{\partial \omega}{\partial t} + \frac{\partial (\overline{u}_j \omega)}{\partial x_j} = \alpha \frac{\omega}{k}\tau_{ij}\frac{\partial \overline{u}_i}{\partial x_j} - \beta\omega^2 + \frac{\sigma_d}{\omega}\frac{\partial k}{\partial x_j}\frac{\partial \omega}{\partial x_j} + \frac{\partial}{\partial x_j}\left[\left(\nu + \sigma \frac{k}{\omega}\right)\frac{\partial \omega}{\partial x_j}\right], \tag{4}$$

with, k the turbulent kinetic energy and ω the specific dissipation rate. The motivation for the modification of the destruction term in (3) is that the dissipation in the k-ω RANS model is $\varepsilon = \beta^* k\omega = k^{3/2}/L_t$, where the turbulent length scale is $L_t = k^{1/2}/(\beta^*\omega)$. So, it means that in the dissipation term, the turbulent length scale is replaced by the grid size. The choice of the grid size measure is crucial in any LES like formulation (Scotti et al., 1993, Spalart et al., 2006, Fröhlich and von Terzi, 2008). The literature shows that there is a preference for the maximum size in a DES formulation (Yan et al., 2005, Spalart et al., 2006), while there is a preference for the cube root measure in a LES formulation (Scotti et al., 1993, Fröhlich and von Terzi, 2008). For the length scale in the k-equation (3), we take the maximum size $\Delta = \max(\Delta_x, \Delta_y, \Delta_z)$, where Δ_x, Δ_y, Δ_z denote the distances between the cell faces in x, y and z directions, in the style as first proposed by Strelets (2001). The closure coefficients and some additional relations are:

$$\beta^* = 0.09, \quad \alpha = 0.52, \quad \beta = \beta_0 f_\beta, \quad \beta_0 = 0.0708,$$
$$\sigma = 0.5, \quad \sigma^* = 0.6, \quad \sigma_{do} = 0.125$$
$$f_\beta = \frac{1+85\chi_\omega}{1+100\chi_\omega}, \quad \chi_\omega = \left|\frac{\Omega_{ij}\Omega_{jk}S_{ki}}{(\beta^*\omega)^3}\right|,$$
$$\sigma_d = \begin{cases} 0 & for \quad \frac{\partial k}{\partial x_j}\frac{\partial \omega}{\partial x_j} \le 0 \\ \sigma_{do} & for \quad \frac{\partial k}{\partial x_j}\frac{\partial \omega}{\partial x_j} > 0 \end{cases}$$

where $\Omega_{ij} = 1/2(\partial U_i/\partial x_j - \partial U_j/\partial x_i)$ is the vorticity tensor.

The eddy-viscosity is defined by (Kok et al., 2004) as

$$\nu_t = \min\left(\frac{k}{\omega}, \beta^* C_{DES}\sqrt{k}\Delta_{LES}\right) \tag{5}$$

where $\Delta_{LES} = (\Delta_x\Delta_y\Delta_z)^{1/3}$. The motivation for this modification is that the RANS eddy viscosity is $\nu_t = \beta^* L_t \sqrt{k}$. So, it means that also in the eddy viscosity expression, the turbulent length scale is replaced by the grid size. The chosen grid size is here the cube root measure, so the typical LES grid size. The grid size is multiplied with the tuning constant C_{DES}. The justification for using different grid scales in Eq. (5) and in the k-equation (Eq. 3) is given below.

Under local equilibrium (production of k equal to dissipation of k), the eddy viscosity reduces in LES mode to a Smagorinsky subgrid viscosity (S is the magnitude of the shear rate tensor):

$$\nu_t = \left((\beta^*)^{3/4} C_{DES}\Delta_{LES}\left(\frac{\Delta}{\Delta_{LES}}\right)^{1/4}\right)^2 S. \tag{6}$$

The role of the term $(\Delta/\Delta_{LES})^{1/4}$ is to increase the eddy viscosity on high aspect ratio cells, with respect to the value obtained by the cube root grid size in all turbulence length scale substitutions, as in the model by Scotti et al. (1993), which improves the predictive qualities of LES on anisotropic grids. In Eq. (6), the Smagorinsky constant $C_s = (\beta^*)^{3/4} C_{DES}$ is set to the usual value 0.1, which gives $C_{DES} = 0.6086$.

For the RANS simulations (Wilcox, 2008), a stress limiter is applied. This means that the turbulent viscosity ν_t is defined by

$$\nu_t = \frac{k}{\tilde{\omega}}, \quad \tilde{\omega} = \max\left(\omega, C_{\lim}\sqrt{\frac{2S_{ij}S_{ij}}{\beta^*}}\right) \tag{7}$$

with $C_{lim} = 7/8$. The RANS stress limiter (Wilcox, 2008) is omitted in Eq. (5) in the hybrid RANS/LES model.

At the walls, k and ω are set to

$$k = 0, \quad \omega = u_\tau^2 / \nu \; S_R, \tag{8}$$

where $S_R=\min[(200/k_s^+)^2, 6/(\beta_0(\Delta y^+)^2)]$, $\Delta y^+=\Delta y \cdot u_\tau/\nu$, $u_\tau=(\tau_w/\rho)^{1/2}$, $\tau_w=\mu \cdot S$ and k_s^+ is a dimensionless roughness height. According to Wilcox (2008), at smooth surfaces, the dimensionless roughness height k_s^+ is less than 5. The walls are assumed to be hydraulically smooth, so the dimensionless roughness height was set here to 4.

3 Computational aspects

Fig. 1 shows a sketch of the dimension of the computational domain, coordinate system and rotation axis for simulation of the rotating channel flow. The flow is assumed to be periodic in streamwise x-direction. The ribs have a square cross-section with H=8mm.

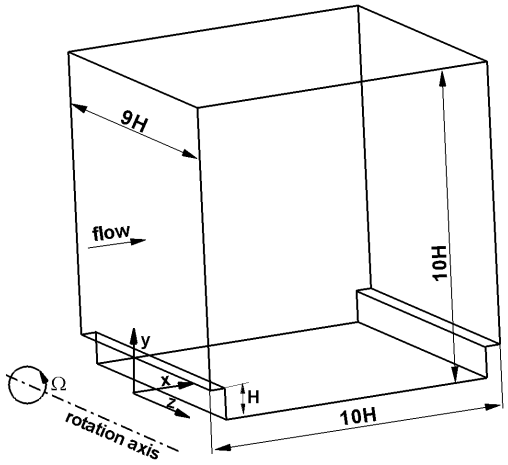

Figure 1: Computational domain, coordinate system and rotation axis for the counter-clockwise rotation. Streamwise periodic conditions are applied in x-direction

The ribbed channel is rotating in counter-clockwise direction around the z-axis (Fig. 1) with the rotation number $Ro=\Omega D_h/U_0$ set to 0.3 (D_h is the hydraulic diameter and U_0 is the bulk streamwise velocity). The clockwise and counter-clockwise rotations of the experiments are studied here, by keeping the coordinate system and the sense of the angular velocity Ω as in Fig. 1, but by turning the computational domain by 180 deg over the x-axis (Fig. 2), in order to obtain the clockwise rotation of the experiments. The Reynolds number based on U_0 and D_h is Re=15,000. Periodic conditions are imposed in the streamwise direction, according to the experiments by Coletti and Arts (2011).

Block-structured grids have been generated. Fig. 2 shows the cross-section through the basic (a) and fine (b) grids for simulation of rib-roughened channel flow in clockwise rotation. The basic and fine grids have about 1 and 4.5 million (M) cells, respectively. The grids have been refined close to the ribbed walls, so the maximum value of y^+ was less than 3. For the hybrid RANS/LES model, the bounded central differencing scheme was applied to the convective terms in the momentum equations. The second order upwind scheme was used for the convective terms in the k- and ω-equations. For RANS, the second order upwind scheme was used for discretisation of the convective terms in all equations. For temporal discretisation, a second-order implicit scheme was applied for both the RANS and hybrid RANS/LES model simulations. An implicit time stepping technique was chosen to guarantee stability for large CFL number. The time step was, however, chosen small enough so that the CFL-number was at maximum 3, so that the dissipation due to the time stepping remained small. In all simulations the time step was set to $\Delta t \cdot V_0/D_h=1.8 \cdot 10^{-3}$. At each time step, inner iteration steps were applied to lower the residuals for the momentum and the transport equations below 10^{-5}. The governing equations were solved sequentially with the pressure-correction SIMPLE method and momentum interpolation was used for the pressure-velocity coupling.

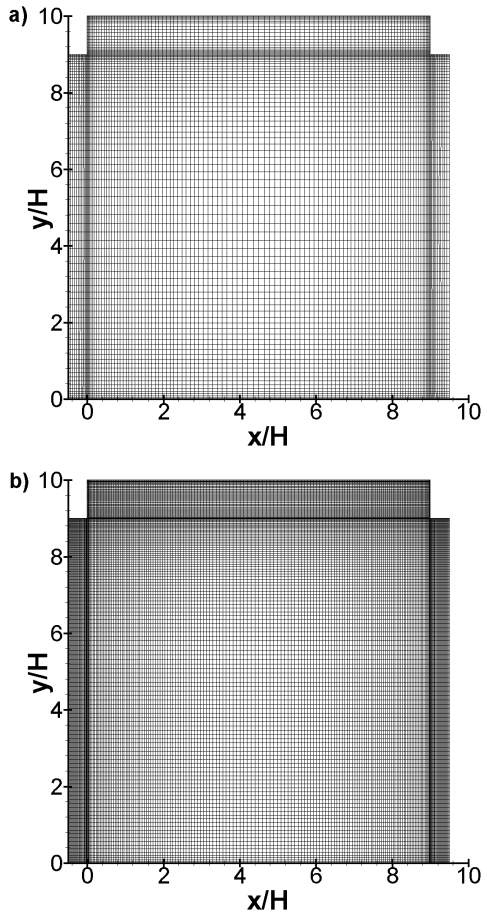

Figure 2: Cross section through the basic (a) and fine (b) grids in the xy-plane for the clockwise rotation.

4. Results

Fig. 3 shows the contour plots of instantaneous streamwise velocity for simulation with the hybrid RANS/LES model in clockwise (a) and counter-clockwise (b) rotation. The clockwise rotation stabilises the flow (Fig. 3 a). The opposite happens for the counter-clockwise rotation (Fig. 3 b).

The Coriolis force weakens the vortical motion in the clockwise rotation case, which gives a larger size of the separation bubble behind the rib, than in the counter-clockwise rotation. The counter-clockwise rotation leads to enhancement of the small-scale turbulent motion inside the channel which makes the recirculation behind the rib a bit smaller with respect to the one observed in the non-rotating case (Coletti and Arts, 2011).

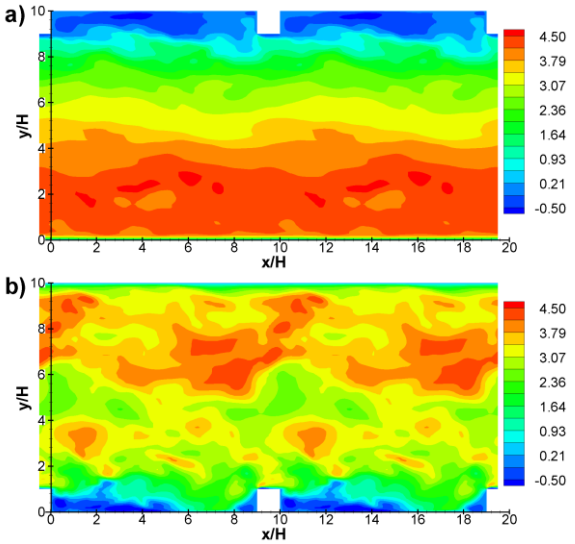

Figure 3: Contour plots of instantaneous streamwise velocity (a) in clockwise and (b) in counter-clockwise rotation obtained with the hybrid RANS/LES model. The flow is from left to right. The computational domain is copied once in the x-direction.

Fig. 4 shows the instantaneous field of $f_{vt}=\min(\nu_t/\nu_{RANS},1)$, (where $\nu_{RANS}=k/\omega$) for simulation on the basic mesh (1M) with clockwise (a) and counter-clockwise (b) rotations and on the fine mesh (4.5M) in clockwise rotation (c) with the hybrid model. The flow regions with $f_{vt}=1$ correspond to the nominal RANS zones. Note that the RANS value is reduced with respect to a true RANS due to the modified source term in the k-equation (Eq. 3). RANS zones are, in principle, active close to walls (Fig. 4). Away from walls the hybrid model turns into the LES mode, but spontaneously some small RANS zones are obtained inside the channel. A closer look to the ribbed walls for the clockwise rotation (Fig. 4 a and c) reveals the narrow LES zones in the near wall region (first two or three cells) in which $f_{vt}=\nu_t/\nu_{RANS}$ is close to zero. This is due to the destabilising effect of the Coriolis force which suppresses the activity of the small-scale dynamics there. There is no significant difference between the contour plots of f_{vt} obtained on the basic and fine grids (Fig. 4 a and c). The role of the RANS zones away from walls is negligible. This can be concluded from Fig. 5 showing the ratio of modelled to molecular viscosity for simulation with the hybrid model on the basic grid in clockwise rotation. The ratio is much lower than 1 inside the channel and it goes to unity close to the bottom wall. Similar levels of ν_t/ν were obtained in the other cases studied here (results not shown here). It means that good quality grids have been generated, so that a majority of the flow dynamics is resolved. The role of the subgrid model is secondary. As it will be shown below, the results obtained with the pure RANS model are different from the results obtained with the hybrid models. It means that a hybrid model adequately reduces the level of the turbulent viscosity toward the subgrid viscosity when the model turns into the LES mode.

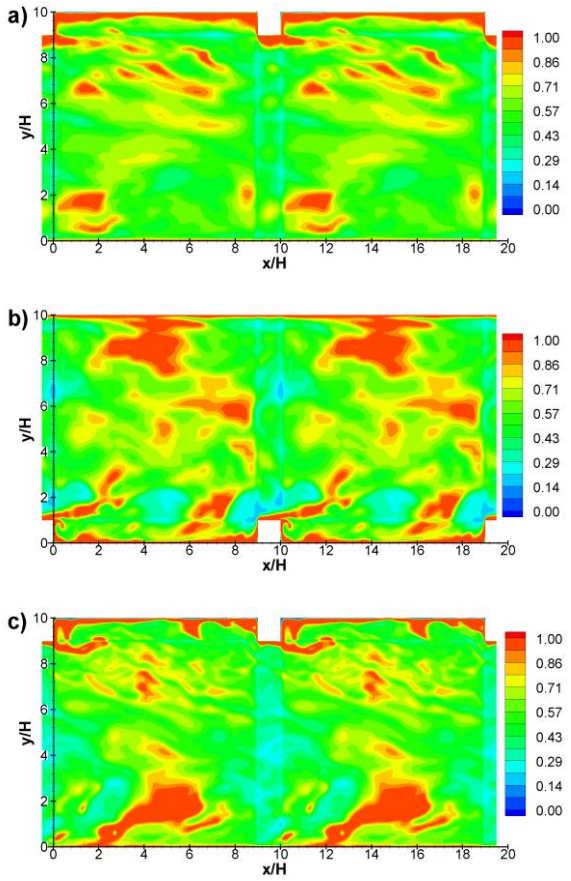

Figure 4: Contour plots of instantaneous field of ν_t/ν_{RANS} (a) in clockwise and (b) in counter-clockwise rotation on the basic mesh and (c) in clockwise rotation on the fine mesh obtained with the hybrid RANS/LES model.

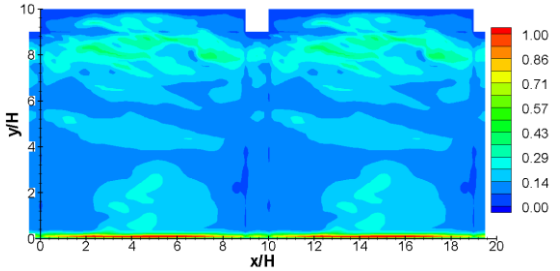

Figure 5: Contour plots of instantaneous field of ν_t/ν for clockwise rotation on the basic mesh.

Mean and total (resolved plus modelled) fluctuating streamwise velocity profiles are shown in Figs. 6 and 7 for both the clockwise and counter-clockwise rotations along the lines perpendicular to the ribbed surface at streamwise distances x/H=0, 2, 4 and 6. The hybrid RANS/LES and RANS (time-accurate) model simulations have been performed on the basic grid with 1M cells. Additionally, the fine grid hybrid RANS/LES model simulations have been performed on the fine mesh (4.5M cells). The size of the separation region is somewhat underpredicted by RANS for the clockwise rotation, as shown in Fig. 6 (b). At the same time, the fluctuating velocity profiles which are reproduced by RANS at distances x/H=2 and x/H=4 (Fig. 7 b and c) are somewhat a too low. It means that for the clockwise rotation the stabilising effect of the Coriolis force, which should lead to stronger momentum loss behind the rib, cannot be fully addressed with the unmodified k-ω model. The results obtained with the hybrid RANS/LES model are in very good agreement with measurements at all locations. The hybrid model results obtained on the fine grid (4.5M) are very similar to the results obtained on the basic grid (1M). This proves grid independency of the hybrid model results. For the counter-clockwise rotation, the RANS model predicts an abrupt separation at the leading side of the rib (Fig. 6 a), which leads to a too high level of fluctuating velocity in the shear layer behind the rib (Fig. 7). In contrast, the streamwise mean velocity profiles are well reproduced with the hybrid RANS/LES model at distances x/H=0, 2 and 4. Some differences are visible between simulations using the hybrid model and experiments close to the channel centre at x/H=6 (Fig. 6 d). The fluctuating velocity profiles are very well reproduced with the hybrid RANS/LES model at x/H=0, 4 and 6 (Fig. 7). Somewhat a too large level of the fluctuating velocity is obtained with the hybrid model at x/H=2. Interestingly, this does not have a negative effect on the mean velocity profiles which are in good agreement with experimental data close to the ribbed surface.

5. Conclusions

Summing up, good results are obtained with the hybrid RANS/LES model for simulation of a rib-roughened rotating channel flow. It means that the hybrid RANS/LES model properly addresses the effect of the Coriolis force on the turbulent flow dynamics, without necessity to include ad hoc corrections to the underlying RANS model. The vortical structures are effectively suppressed outside the separated shear layer behind the rib for the clockwise rotation. Strong vortical motions are well reproduced by the hybrid model inside the channel for the counter-clockwise rotation. It means that the hybrid model can successfully be applied for the study of rib-roughened channel flow on relatively fine grids.

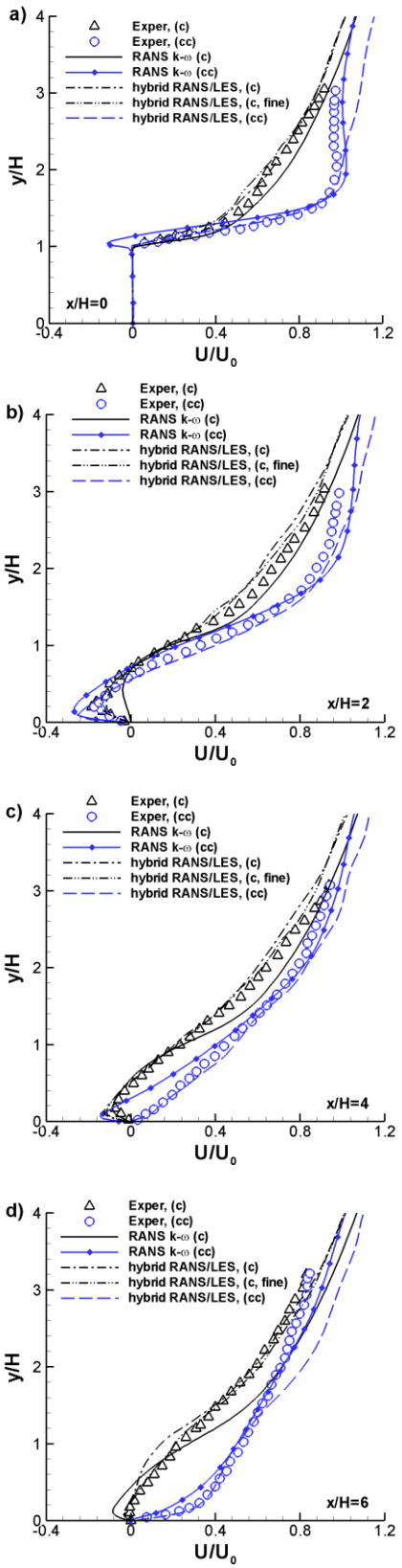

Figure 6: Profiles of mean streamwise velocity along lines perpendicular to the ribbed surface at a) x/H=0, b) x/H=2, c) x/H=4 and d) x/H=6.

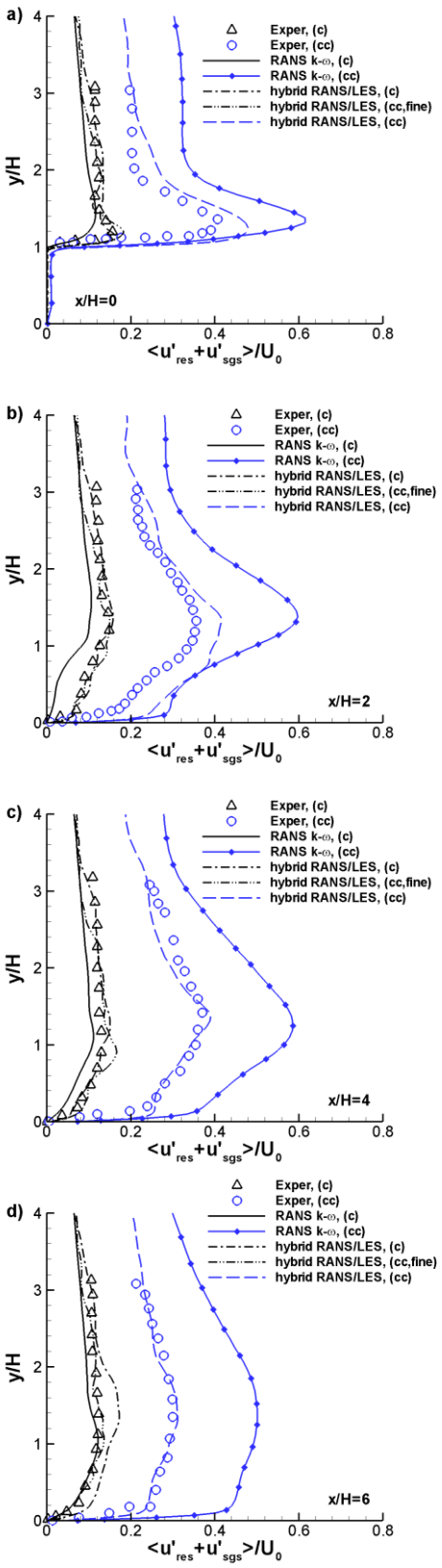

Figure 7: Profiles of total streamwise fluctuating components along lines perpendicular to the ribbed surface at a) x/H=0, b) x/H=2, c) x/H=4 and d) x/H=6.

Acknowledgements

The first author acknowledges an international cooperation grant of Ghent University and the research program 'Iuventus Plus' supported by the Polish Ministry of Science and Higher Education from the National Budget Funds for Science in 2010-2011 (contract number 0211/T02/2010/70).

References

Abdel-Wahab S. and Tafti D.K. (2004), Large eddy simulation of flow and heat transfer in a 90 deg ribbed duct with rotation: Effect of Coriolis and centrifugal buoyancy forces, *J. Turbomachinery*, Vol. 126, pp. 627-636.

Coletti F. and Arts T. (2011), Aerodynamic investigation of a rotating rib-roughened channel by means of time-resolved PIV, 9th European Turbomachinery Conference, Istanbul, Turkey.

Coletti F., Maurer T., Arts T. and Di Sante A. (2010), Flow field investigation in rotating rib-roughened channel by means of particle image velocimetry, 15-th Int. Symp. on Applications of Laser Techniques to Fluid Mechanics, Lisbon, Portugal.

Fröhlich, J and von Terzi, D. (2008), Hybrid LES/RANS methods for the simulation of turbulent flows, *Progress in Aerospace Sciences*, 44, pp. 349–377.

Kok J.C., Dol H., Oskam H. and van der Ven, H. (2004), Extra-large eddy simulation of massively separated flows, AIAA Paper, 2004-0264.

Lohasz M.M., Rambaud P. and Benocci C. (2006), Flow features in a fully developed ribbed duct flow as a Result of MILES, *Flow Turbulence Combust*, Vol. 77, pp. 59–76

Scotti A., Meneveau C. and Lilly D.K. (1993), Generalized Smagorinsky model for anisotropic grids, *Phys. Fluids* A, Vol. 5 No. 9, pp. 2306–2308.

Spalart, P.R., Deck, S., Shur, M.L., Squires, K.D., Strelets, M.Kh. and Travin, A. (2006), A new version of detached-eddy simulation, resistant to ambiguous grid densities, *Theor. Comput. Fluid Dyn.* Vol. 20, pp. 181-195.

Wilcox, D.C., (2008). Formulation of the k-ω turbulence model revisited, AIAA Journal Vol. 46 (11), pp. 2823-2837.

Yan J., Mocket C. and Thiele, F., (2005), Investigation of alternative length scale substitutions in detached-eddy simulation, *Flow Turbulence Combust*, Vol. 74, pp. 85-102.